ASMS

RESEARCH ARTICLE

Consecutive Fragmentation Mechanisms of Protonated Ferulic Acid Probed by Infrared Multiple Photon Dissociation Spectroscopy and Electronic Structure Calculations

Sabrina M. Martens, Rick A. Marta, Jonathan K. Martens, Terry B. McMahon

Department of Chemistry, University of Waterloo, Waterloo, ON, Canada

Abstract

Protonated ferulic acid and its principle fragment ion have been characterized using infrared multiple photon dissociation spectroscopy and electronic structure calculations at the B3LYP/6-311+G(d,p) level of theory. Due to its extensively conjugated structure, protonated ferulic acid is observed to yield three stable fragment ions in IRMPD experiments. It is proposed that two parallel fragmentation pathways of protonated ferulic acid are being observed. The first pathway involves proton transfer, resulting in the loss of water and subsequently carbon monoxide, producing fragment ions m/z 177 and 149, respectively. Optimization of m/z 177 yields a species containing an acylium group, which is supported by a diagnostic peak in the IRMPD spectrum at 2168 cm^{-1}. The second pathway involves an alternate proton transfer leading to loss of methanol and rearrangement to a five-membered ring.

Key words: IRMPD, Ferulic acid, Gas phase fragmentation, Density functional theory, Free electron laser, Ion structure, Vibrational spectra, Energetics

Introduction

Ferulic acid is a derivative of phenylalanine found in plants, which serves to crosslink components of the cell wall giving rise to their rigidity and strength [1–3]. Defense against intrusions such as viruses, insects, and pathogens, in addition to protection against enzymatic hydrolysis, have all been associated with the presence of ferulic acid in the plant cell walls [3]. Due to its reactivity towards free radicals, ferulic acid is a commonly used antioxidant for the prevention of cancer and has also exhibited strong UV absorption capabilities due to its high degree of unsaturation [4–6]. Ferulic acid is also used as a bitterness inhibitor, and is used commercially in order to mask the bitterness of several artificial sweeteners such as saccharin and acesulfame K [7]. Adding ferulic acid to consumable materials also serves to slow lipid peroxidation and consequent spoiling due to oxidation [5].

Experimental and Computational Methods

In the current work, infrared multiple photon dissociation (IRMPD) spectroscopy experiments and electronic structure calculations have been used in order to determine structures and mechanisms associated with the IRMPD fragmentation of protonated ferulic acid. IRMPD, in combination with electronic structure calculations, is a powerful technique for structural elucidation studies such as this [8–30]. IRMPD spectroscopy experiments were

Correspondence to: Sabrina Martens; *e-mail:* s2marten@uwaterloo.ca, Terry McMahon; *e-mail:* mcmahon@uwaterloo.ca
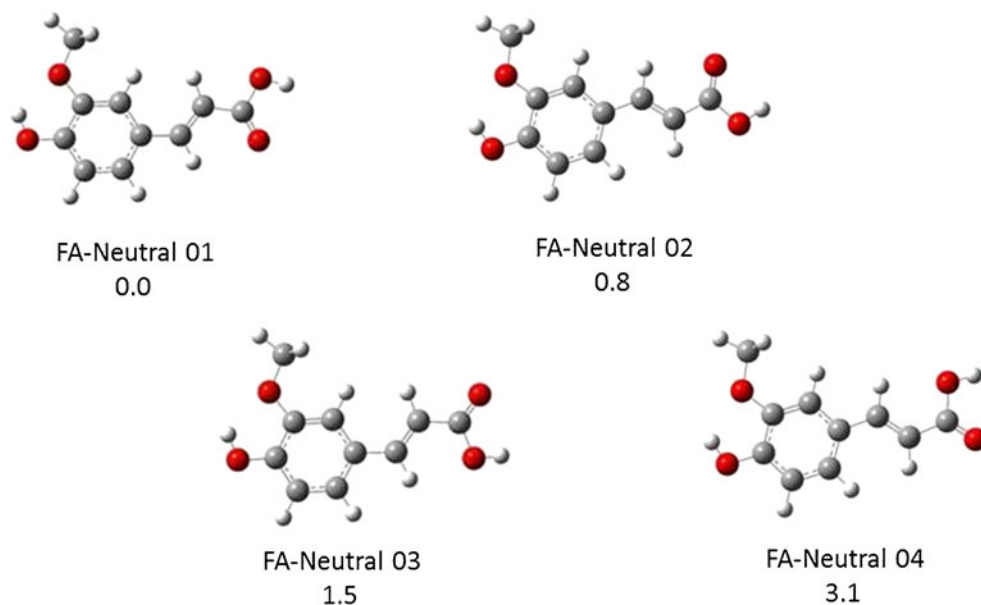
Figure 1. The calculated neutral isomers of ferulic acid with relative Gibbs free energies (298 K) reported in kJ mol^{-1}

performed at the Centre de Laser Infrarouge d'Orsay (CLIO) and have been described in detail previously [8, 12, 13, 24, 31]. The IR-FEL beam was directed into a Bruker (Bruker; 40 Manning Road, Billerica, MA, USA 01821) Esquire 3000+ ion-trap mass spectrometer, equipped with an electrospray ionization interface. Solutions (~10^{-6} M) of protonated ferulic acid were prepared by dissolving solid ferulic acid in a 1:1 mixture of acetonitrile and water, and a small amount of formic acid. These solutions were then electrosprayed into the ion trap mass

spectrometer. The IR-FEL beam is created by emission from a 10–50 MeV electron beam that passes through the gap between a set of periodic undulator magnets. By adjusting the undulator gap, the emission photon wavelength is able to be tuned through the mid-infrared range. The work described here involved the use of electron energies of 46 MeV, which would typically permit continuous scans over a frequency range of 1000–2000 cm^{-1}; however, in one case described below, scans of up to a frequency of 2168 cm^{-1} were obtained in order to detect the presence of an acylium stretch.
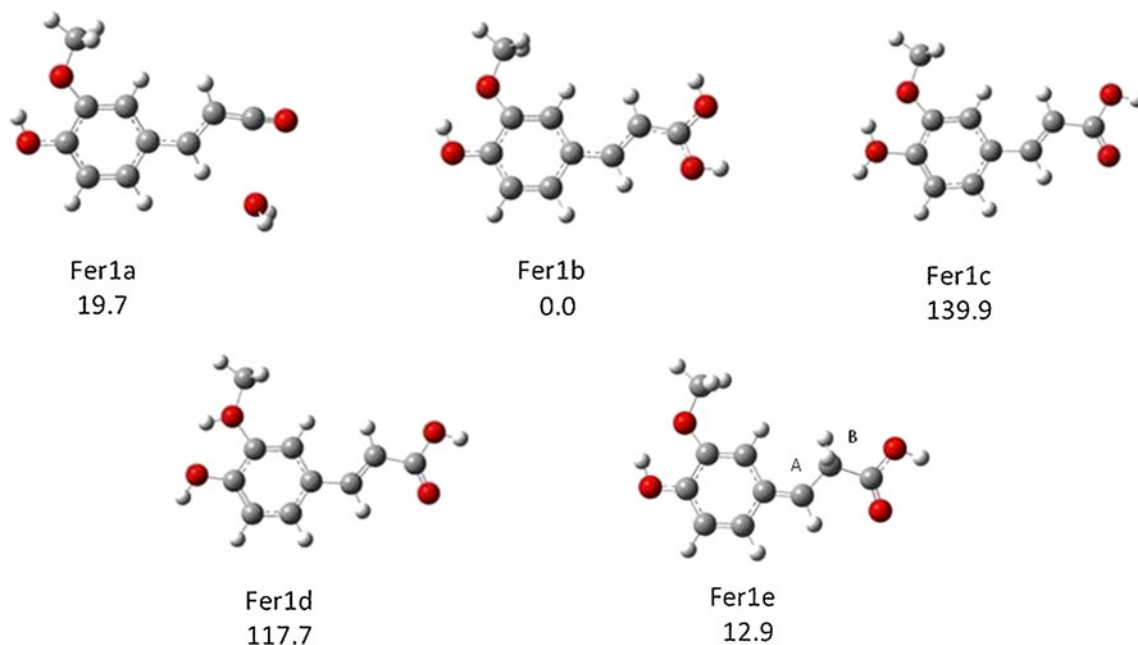

Figure 2. The lowest energy calculated isomers for each potential site of protonation on ferulic acid. For isomer Fer1e, protonation at both carbons A and B was considered, but protonation at site A results in a proton transfer to site B, yielding Fer1e. Relative Gibbs free energies (298 K) are reported in kJ mol^{-1}

Table 1. The Proton Affinities (PA) and Gas Basicities (GB) (298 K) Associated with Protonation of the Heteroatom Sites A Through E of Neutral Ferulic Acid in kJ mol^{-1}, Calculated at the B3LYP/6 − 311 + G(d,p) Level of Theory
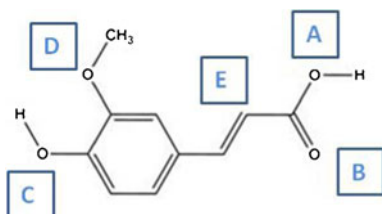
Site	Isomer	PA	GB
A	Fer1a	860	843
B	Fer1b	896	863
C	Fer1c	746	723
D	Fer1d	774	745
E	Fer1e	879	850

Electronic structure calculations have been performed using the Gaussian 09 software package [32]. All geometry optimizations and associated frequency calculations have been performed at the B3LYP/6-311+G(d,p) level of theory, which has been shown to be a reliable protocol, with a good compromise between accuracy and cost, for smaller systems such as those described here [13, 14, 16, 24, 33–36]. All harmonic frequencies obtained at this level of theory were scaled by 0.9679 [37] in order to compensate for errors arising from the use of a harmonic oscillator approximation in calculating the frequencies, as well as long range electron correlation effects.

Anharmonic frequencies [38] have also been obtained at the B3LYP/6-311+G(d,p) level of theory for all species considered to be the most chemically significant. Since real molecules exhibit naturally anharmonic vibrations, it can be
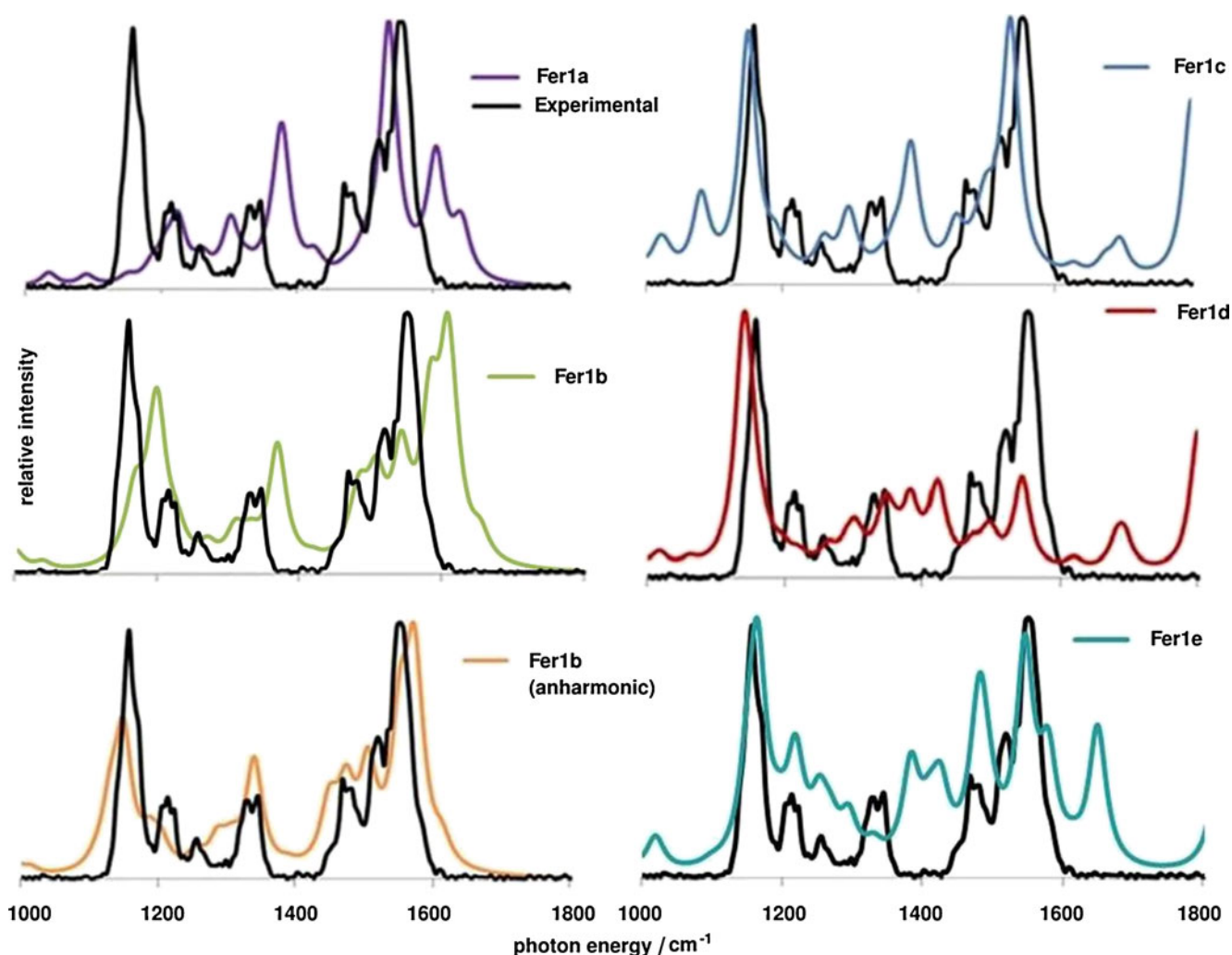

Figure 3. A comparison of the experimental spectrum with each of the lowest energy calculated (harmonic) spectra for ferulic acid protonated at sites A through E. The experimental spectrum is shown in black and the calculated spectra in color. Spectra were calculated at the B3LYP/6-311 + G(d,p) level of theory

useful, though sometimes computationally costly, to obtain anharmonic frequencies. Here the use of calculated anharmonic frequencies greatly improves the fit between the IRMPD spectra obtained and the computational results in all cases. The anharmonic frequency calculation is useful for reproducing the spectral range of 1000 to 2200 cm^{-1} found in this work. It is well established that the harmonic fundamental frequencies determined by ab initio and DFT SCF methods overestimate experimental fundamental frequencies for typical, covalently bound molecules by 8 % to 12 % [39]. The reasons for such deviations include basis set incompleteness, electron correlation effects, and anharmonicity [39]. The anharmonic potential requires the calculation of third and fourth order partial derivatives, which are the anharmonic force constants for the cubic and quartic terms, respectively. It is the calculation of these higher order partial derivatives that cause evaluation of anharmonic frequencies to be substantially more costly than harmonic frequencies. In many cases, the cubic and quartic potentials are treated as a perturbation to the harmonic oscillator potential [39]. Computed vibrational spectra were generated using a Lorentzian line shape with a full width at half maximum of 15 cm^{-1}.

Discussion

Several isomers of neutral ferulic acid have been calculated and four are shown below in Figure 1. FA-Neutrals 01, 02, 03, and 04 have been calculated to be the most favorable isomers based on their relative Gibbs free energies (298 K), and in each, the hydrogen attached to the OH of the carboxylic acid group is directed away from the side chain sp^2 hydrogen atoms, minimizing steric interactions.

Since protonated ferulic acid is being observed in the IRMPD experiments, it is important to first consider the most likely site of protonation on neutral ferulic acid. Electronic structure calculations in combination with the IRMPD spectrum of protonated ferulic acid have been used in order to determine if protonation occurs at the carbonyl or hydroxyl oxygens of the acid functional group, the methoxy group, across the double bond, or the phenolic group. Several isomers were calculated for each potential site of protonation and a lowest energy isomer for each is shown below in Figure 2. The proton affinities (PA) and gas basicities (GB) of the different Lewis basic heteroatoms found in FA-Neutral 01 are reported in Table 1.

The IRMPD spectrum for protonated ferulic acid strongly indicates that the initial site of protonation occurs on the carbonyl oxygen. The harmonic calculated spectrum for isomer Fer1b is found to best match the experimental spectrum compared with calculated spectra corresponding to other sites of protonation (Figure 3). The anharmonic calculated spectrum of isomer Fer1b is comparatively redshifted relative to its harmonic spectrum, further improving the match between the calculated and experimental spectra of Fer1b. Characteristic peaks resulting from the asymmetric

Table 2. Peak Assignments for Isomer Fer1b of m/z 195

Peak Assignments (cm^{-1})		
Harmonic	Anharmonic	Description
1167, 1199	1130, 1149	C(OH)$_2$$^+$ rocking
1369	1339	Phenolic stretch
1509	1474	Methoxy scissoring
1610	1572	Rocking of the phenolic and acid OH groups

rocking of the two hydroxy groups in the C(OH)$_2$$^+$ functionality are located at 1199, 1149, and 1157 cm^{-1}, for the calculated harmonic, calculated anharmonic, and experimental spectra, respectively. The calculated anharmonic spectrum matches the experimental spectrum very closely, largely supporting that the carbonyl protonated species is being observed in the experiment.

The harmonic calculated spectra corresponding to isomers Fer1a, Fer1c, Fer1d, and Fer1e each show diagnostic peaks which are characteristic of their conformations, but differ from the experimental spectrum (Figure 3). The calculated spectrum of Fer1d has such a peak at 1421 cm^{-1}, which results from the proton rocking on the methoxy group. In addition to this, there is the beginning of a large peak at 1801 cm^{-1} that corresponds to the stretching mode of a free carbonyl. This signature is not present in the experimental spectrum, further indicating that the carbonyl oxygen is the site of protonation. For isomer Fer1a, the large peak at 1150 cm^{-1} in the experimental spectrum is not accounted for in the simulated spectrum. This missing peak corresponds to rocking of the hydroxyl in the COOH group which, in isomer Fer1a, is protonated to form water. Because protonation at this site forms water which can then dissociate without barrier, a vibrational signature indicative of a carbonyl group is not exhibited by this species. The calculated spectrum of Fer1c however, does show the beginning of a carbonyl peak at 1800 cm^{-1}, since this species does not involve protonation of either of the hydroxyl or carbonyl oxygen atoms, but protonation of the phenolic oxygen. The spectrum of Fer1c also has peaks at 1027 and 1535 cm^{-1}, resulting from the rocking and bending of the R$-$$^+OH_2$ hydrogens, respectively. Another peak calculated to occur at 1080 cm^{-1} arises from the C$-$O stretch of the R$-$$^+OH_2$ group; however, this signature is not observed in the

Table 3. Calculated Relative Energetics for the Lowest Energy m/z 195 Isomers Corresponding to Each Site of Protonation. Values were Calculated at the B3LYP/6$-$311+G(d,p) Level of Theory and are Reported in kJ mol^{-1} for $\Delta G_{rel}°$ and $\Delta H_{rel}°$ and in J mol^{-1} K^{-1} for $\Delta S_{rel}°$

Isomer	Site of Protonation	$\Delta H_{rel}°$	$\Delta S_{rel}°$	$\Delta G_{rel}°$
Fer1a	A	35.3	$-$52.6	19.7
Fer1b	B	0.0	0.0	0.0
Fer1c	C	149.6	$-$32.7	139.9
Fer1d	D	122.0	$-$14.5	117.7
Fer1e	E	16.4	$-$11.6	12.9

IRMPD spectrum. Isomer Fer1e corresponds to protonation on the double bond of the carboxylic acid-containing side chain. Protonation at both carbon atom A and B of the double bond was calculated (labeled in Figure 2); however, during the optimization process, protonation at carbon A resulted in a proton transfer to carbon B, yielding a single protonated species. The spectrum of Fer1e shows the beginning of a carbonyl peak in the 1800 cm^{-1} region, since in this isomer a carbonyl is present. In addition to this, there is an extra peak located at 1651 cm^{-1}, not found in the experimental spectrum,
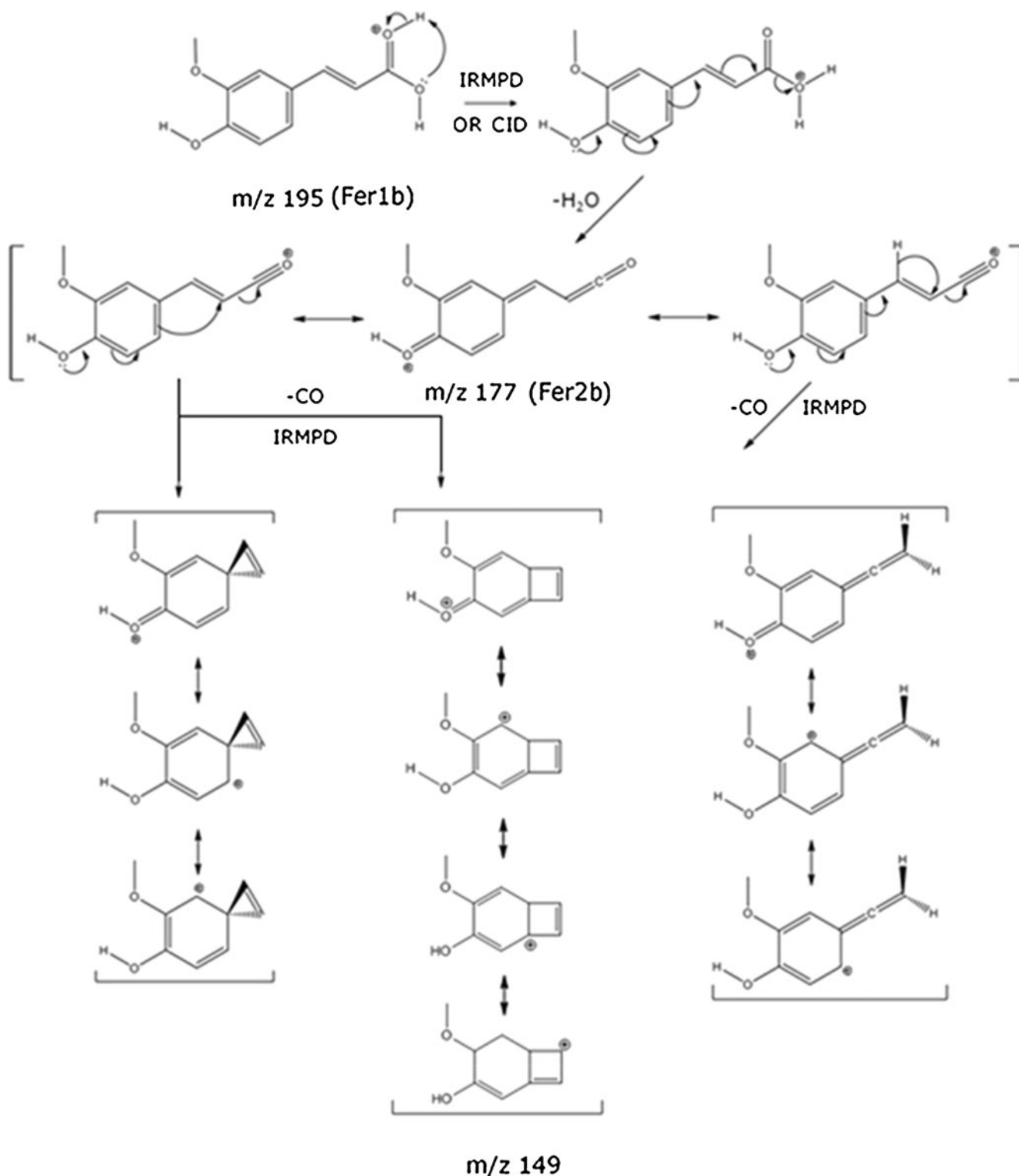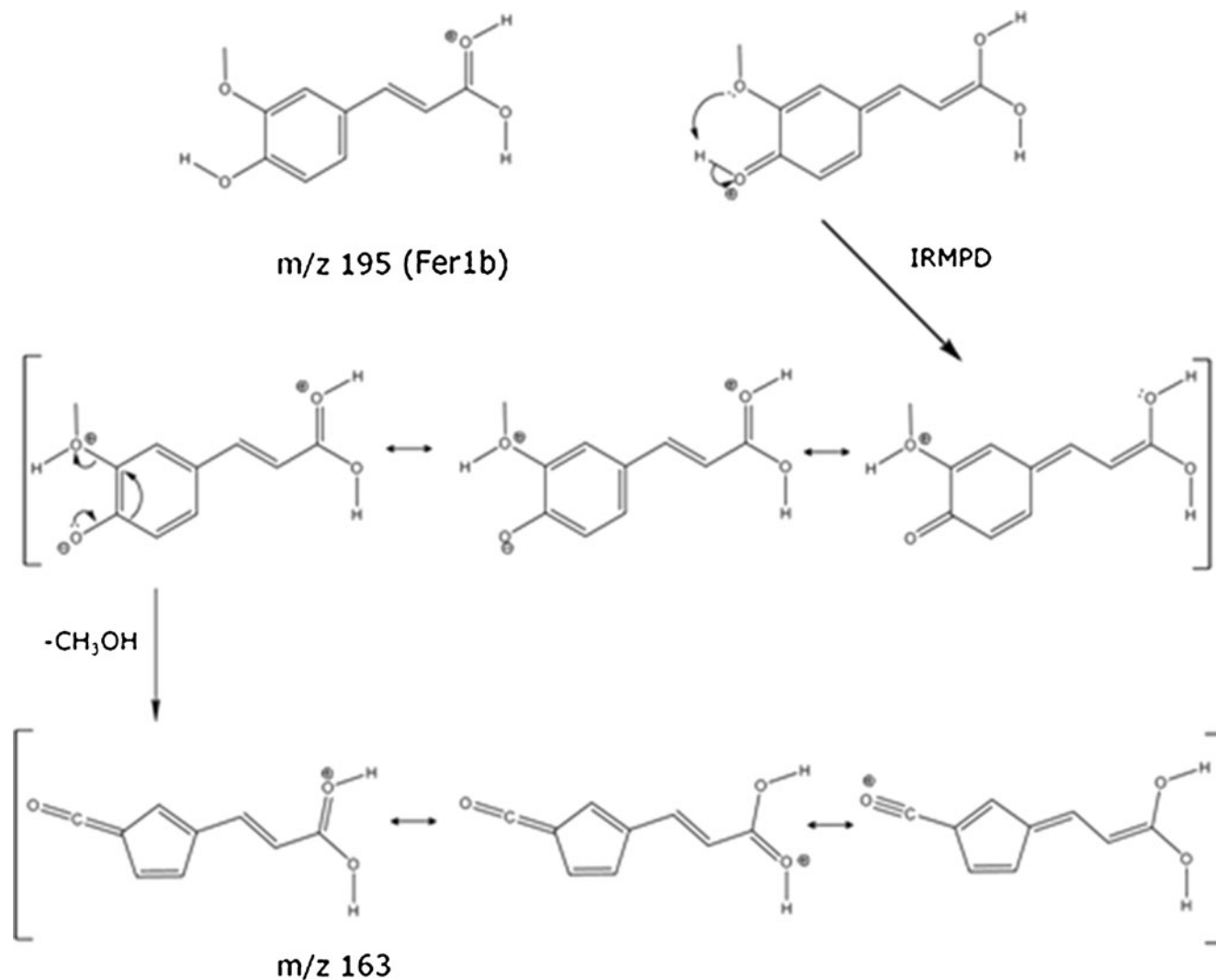

Scheme 1. The proposed mechanism for the formation of the ions of *m/z* 177 and 149; initiated by proton transfer, leading to the loss of water and subsequent loss of carbon monoxide

corresponding to the stretching of the double bonds, which in this isomer are conjugated through the ring and chain. A peak at 1384 cm^{-1} in the calculated Fer1e spectrum corresponds to the rocking of the hydrogens on the site of protonation, which is not represented in the experimental spectrum. Therefore, considering these differences, the calculated spectrum of Fer1b matches the experimental spectrum most closely. Peak assignments for Fer1b are listed in Table 2.

In addition to spectral comparisons, isomer Fer1b has been calculated to be the lowest energy isomer for protonated ferulic acid based on the relative Gibbs free energies (298 K) for a number of isomers for each potential site of protonation. Based on the calculated Gibbs free energies (298 K) of additional isomers, it is found that ferulic acid is consistently lowest in energy when the majority of the atoms lie in a single plane, with the exception of two of the methyl hydrogen atoms of the methoxy group. Relative thermochemical values (298 K) of the lowest energy isomer for each potential

site of protonation on ferulic acid can be found in Table 3. Isomer Fer1b, corresponding to protonation on the carbonyl oxygen, has been calculated to be approximately 20 kJ mol^{-1} lower in Gibbs free energy (298 K) than the hydroxyl protonated species, and approximately 13 kJ mol^{-1} lower than protonation at the double bond, which is the next lowest energy structure found. Therefore, based on both spectra and energetics, it is expected that neutral ferulic acid is primarily protonated on the carbonyl oxygen.

Protonation on the carbonyl oxygen has been calculated to be most favorable; however, in addition to isomer Fer1b, there are two other energetically relevant isomers corresponding to protonation at this site, shown in the supplementary data. Based on the relative Gibbs free energies (298 K) of these isomers, Fer1b is likely the most abundant isomer of protonated ferulic acid; however, the other isomers shown may also be present to some extent.

Scheme 2. The proposed mechanism of formation for the ion of *m/z* 163; initiated by a proton transfer, followed by the loss of methanol

Because of its extensively conjugated structure, protonated ferulic acid has been observed to undergo very interesting fragmentation in IRMPD spectroscopy experiments, since several stable fragment ions can be formed. Following IRMPD, protonated ferulic acid (*m/z* 195) gives rise to three fragment ions that can be observed simultaneously. Detailed mechanisms for several fragmentation processes are proposed and are shown in Schemes 1 and 2.

Through proton transfer and endothermic loss of water (35.6 kJ mol^{-1}), protonated ferulic acid forms a fragment ion of *m/z* 177, which can be considered a resonance hybrid between acylium ($-C\equiv O^+$) and ketene ($-C^+=C=O$) structural moieties. Several starting structures of the ion of *m/z* 177 were considered, however, all calculated isomers converged to two isomers, Fer2a and Fer2b. Fer2a and Fer2b are shown in Figure 4 along with their relative Gibbs free energies reported in kJ mol^{-1}.

These two species are geometric isomers and based on their relative Gibbs free energies (298 K) differing by only 1.5 kJ mol^{-1}, both species will likely be present in experiment. Comparisons of the calculated and experimental spectra corresponding to Fer2a and Fer2b are shown in Figure 4. Further spectral analysis will be based upon isomer Fer2b as the spectra and energetics obtained for Fer2a and Fer2b are effectively analogous. The harmonic calculated spectrum of isomer Fer2b has a peak at 1221 cm^{-1} corresponding to rocking of the phenolic and methoxy groups. Stretching of the sp^2 carbons in the molecule gives rise to a peak at 1535 cm^{-1} and the large diagnostic peak located at 2260 cm^{-1} results from the stretching motion of the acylium moiety. These peaks are located, respectively, at 1192, 1494, and 2220 cm^{-1} in the calculated anharmonic spectrum and at 1201, 1474, and 2168 cm^{-1} in the experimental spectrum. The anharmonic spectrum of Fer2b is found to be red-shifted relative to the calculated harmonic spectrum and to match the IRMPD spectrum more closely. This seems reasonable since the vibrational modes in this molecule are likely more anharmonic in nature due to the extensive conjugation of the atoms in protonated ferulic acid. Calculated bond lengths for *m/z* 177 (Figure 4) indicate that the acylium ion structure is most representative of the resonance hybrid [40]. Therefore, based on the analysis of both spectra and energetics, Fer2b (in combination with Fer2a) is most likely the species being observed experimentally.

Following IRMPD, ion *m/z* 177 subsequently loses carbon monoxide to form a fragment of *m/z* 149. In order to probe the structure and mechanism of formation of this product, *m/z* 177 was formed by collision induced dissociation (CID) and subsequently subjected to IRMPD. Presuming that the *m/z* 177 formed by CID is identical to that resulting from IRMPD, the subsequent loss of CO can be considered [41–43]. Three possible isomers for ion *m/z* 149 have been proposed and are shown in Scheme 1. However, due to the significant ring strain present in the three and four-membered ring
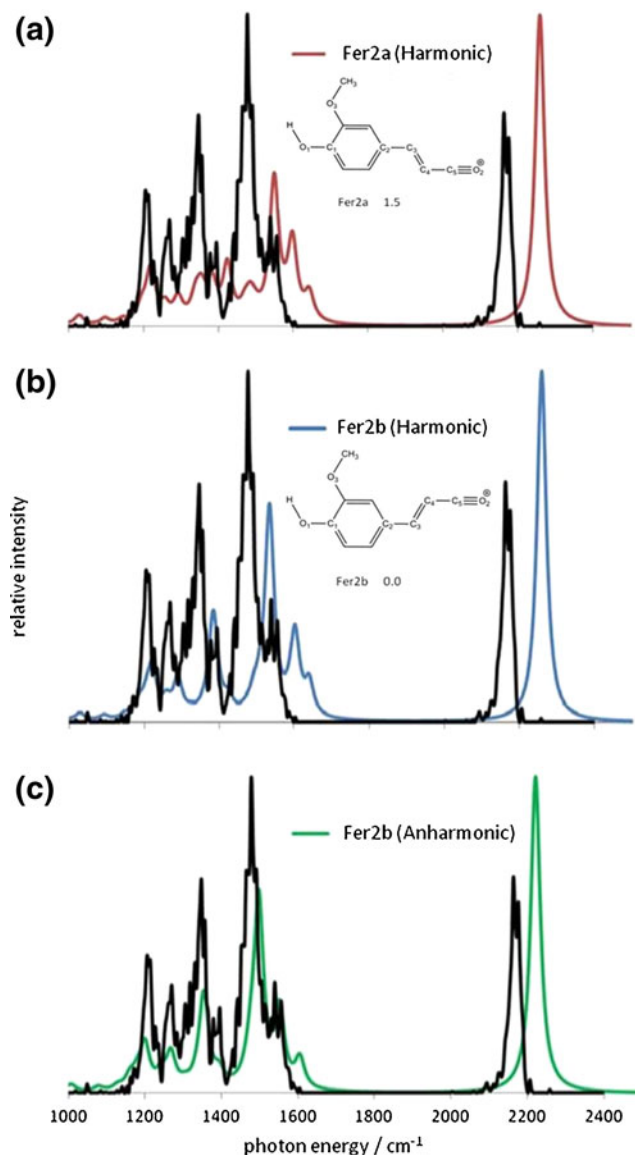

Figure 4. A comparison of the lowest energy calculated harmonic (above) and anharmonic (below) vibrational spectra and the experimental IRMPD spectrum for ion *m/z* 177. IRMPD intensities are in relative units of fragmentation efficiency and calculated intensities are in relative units of km mol^{-1}

containing structures, the allene-type structure is the most energetically favorable, and therefore the most likely species being observed in experiment. The relative Gibbs free energies (298 K) of the two less favorable isomers are approximately 100 kJ mol^{-1} higher and their structures and energetics are shown in Scheme 1 and Table 4, respectively. Additionally, an isomer containing an eight-membered ring was considered; however, upon optimization, the eight-membered ring collapsed to a four-membered ring. Simple bond cleavage of *m/z* 177, resulting in the loss of CO, thus gives rise to an allene-like structure for *m/z* 149. Ideally, the structure of *m/z* 149 would also have been probed by IRMPD, however, there was insufficient intensity for this

Table 4. Relative Energetics for the Three Calculated m/z 149 Isomers Reported in kJ mol^{-1} for $\Delta H_{rel}°$ and $\Delta G_{rel}°$, and in J mol^{-1} K^{-1} for $\Delta S_{rel}°$. Values Have Been Calculated at the B3LYP/6−311+G(d,p) Level of Theory

Isomer	$\Delta H_{rel}°$	$\Delta S_{rel}°$	$\Delta G_{rel}°$
Fer3a	105.8	−7.8	108.2
Fer3b	105.6	−14.5	109.9
Fer3c	0.0	0.0	0.0

fragment to make it feasible. Calculated bond lengths for m/z 149, corresponding to Fer3c, are listed in Table 5.

A second, independent, fragmentation pathway also exists in which protonated ferulic acid undergoes loss of methanol to form an ion of m/z 163. Since direct protonation on the methoxy group is quite unfavorable, it is likely that proton transfer takes place. The potential for intramolecular proton transfer from the C(OH)$_2^+$ group of the side chain by forming a "scorpion-like" tail was

considered and a corresponding structure was successfully optimized ($\Delta G_{rel}°$=48.5 kJ mol^{-1} compared with Fer1b for m/z 195). It was found, however, that such a proton transfer could not be facilitated since the proximity between the oxygen of the methoxy group and a proton from the C(OH)$_2^+$ group is found to be 3.95 Å. Therefore, proton transfer presumably occurs due to transfer of the phenolic proton to the adjacent methoxy group.

Following proton transfer, a concerted rearrangement of the phenyl ring leads to formation of a five-membered ring, accompanying the loss of methanol. All attempts to find a six-membered ring structure led spontaneously to collapse to the five-membered ring structure. The proposed structure and bond lengths of the five-membered ring species are shown in Table 5. The bond lengths indicate that the resonance hybrid of m/z 163 is best represented by an acylium-type structure. The proposed mechanism for formation of m/z 163 is shown in Scheme 2.

Table 5. The Calculated Bond Lengths (Å) for the Proposed Structures of: m/z 177 (top), which is in Resonance Between an Acylium and Ketene Type Species, the Allene-Containing Structure of m/z 149 (middle), and m/z 163 (bottom), Which is in Resonance Between a Ketene and Acylium Type Species, and Contains a Five-Membered Ring

Bond	Bond Length
O1 – C1	1.32
C2 – C3	1.40
C3 – C4	1.40
C4 – C5	1.35
C5 – O2	1.14
C8 − O3	1.35
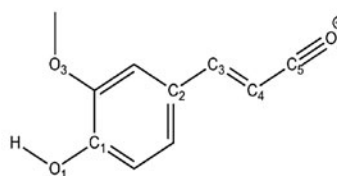
m/z 177

Bond	Bond Length
O1 – C1	1.31
C1 – C2	1.41
C2 – C3	1.37
C3 – C4	1.44
C4 – C5	1.35
C5 – C6	1.29
C4 – C7	1.44
C7 – C8	1.37
C8 – C1	1.44
C8 − O2	1.35
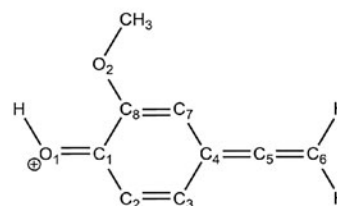
m/z 149

Bond	Bond Length
O1 – C1	1.14
C1 – C2	1.35
C2 – C3	1.42
C3 – C4	1.41
C4 – C5	1.41
C5 – C6	1.39
C6 – C7	1.39
C7 – O2	1.31
C7 – O3	1.32
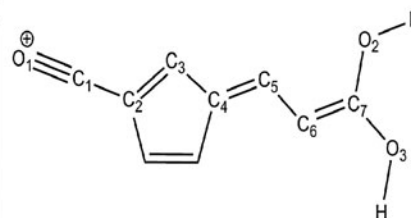
m/z 163

Conclusions

In summary, IRMPD spectroscopy has shown that protonated ferulic acid produces three fragment ion peaks (m/z 177, 149, and 163). The experimental IRMPD spectrum of this extensively conjugated species is matched exceptionally well by the anharmonic spectrum calculated at the B3LYP/6-311+G(d,p) level of theory. Protonated ferulic acid (m/z 195) has been observed to undergo two unique fragmentation mechanisms during IRMPD experiments. Schemes 1 and 2 both show that ferulic acid as being initially protonated on the carbonyl oxygen. Scheme 1 shows that following IRMPD, proton transfer from the carbonyl to the hydroxyl oxygen results in the loss of water yielding an ion of m/z 177. Further isolation of the ion of m/z 177 followed by IRMPD results in the loss of carbon monoxide to form an allene-type ion of m/z 149. Scheme 2 shows that proton transfer from the phenolic OH to the adjacent methoxy group occurs, resulting in the loss of methanol and rearrangement to form a five-membered ring. This work has again demonstrated that IRMPD spectroscopy, coupled with electronic structure calculations, can be a powerful technique for determining the mechanism of dissociation and the structure of ions in the gas phase.

Acknowledgments

References

1. Mathew, S., Abraham, T.E.: Ferulic Acid: an antioxidant found naturally in plant cell walls and feruloyl esterases involved in its release and their applications. *Crit. Rev. Biotechnol.* **24**, 59–83 (2004)
2. Iiyama, K., Lam, T.B.T., Stone, B.A.: Covalent cross-links in the cell wall. *Plant Physiol.* **104**, 315–320 (1994)
3. Casolaro, M., Anselmi, C., Picciocchi, G.: The protonation thermodynamics of ferulic acid/[gamma]-cyclodextrin inclusion compounds. *Thermochim. Acta* **425**, 143–147 (2005)
4. Kikuzaki, H., Hisamoto, M., Hirose, K., Akiyama, K., Taniguchi, H.: Antioxidant properties of ferulic acid and its related compounds. *J. Agric. Food Chem.* **50**, 2161–2168 (2002)
5. Graf, E.: Antioxidant potential of ferulic acid. *Free Radic. Biol. Med.* **13**, 435–448 (1992)
6. Maurya, D.K., Devasagayam, T.P.A.: Antioxidant and pro-oxidant nature of hydroxycinnamic acid derivatives ferulic and caffeic acids. *Food Chem. Toxicol.* **48**, 3369–3373 (2010)
7. Riemer, J.A.: Bitterness inhibitors. United States Patent. Kraft General Foods, Inc., USA (1993)
8. Marta, R.A., Wu, R.H., Eldridge, K.R., Martens, J.K., McMahon, T.B.: The sodium cation-bound dimer of theophylline: IRMPD spectroscopy of a highly symmetric electrostatically bound species. *Int. J. Mass Spectrom.* **297**, 76–84 (2010)
9. Schafer, M., Drayss, M.K., Blunk, D., Purcell, J.M., Hendrickson, C.L., Marshall, A.G., Mookherjee, A., Armentrout, P.B.: Kinetic determination of potassium affinities by IRMPD: elucidation of precursor ion structures. *J. Phys. Chem. A* **113**, 7779–7783 (2009)
10. O'Brien, J.T., Prell, J.S., Berden, G., Oomens, J., Williams, E.R.: Effects of anions on the zwitterion stability of Glu, His, and Arg investigated by IRMPD spectroscopy and theory. *Int. J. Mass Spectrom.* **297**, 116–123 (2010)
11. Dunbar, R.C., Steill, J.D., Oomens, J.: Cationized phenylalanine conformations characterized by IRMPD and computation for singly and doubly charged ions. *Phys. Chem. Chem. Phys.* **12**, 13383–13393 (2010)
12. Wu, R., Marta, R., Martens, J., Eldridge, K., McMahon, T.: Experimental and theoretical investigation of the proton-bound dimer of lysine. *J. Am. Soc. Mass Spectrom.* **22**, 1651–1659 (2011)
13. Martens, S.M., Marta, R.A., Martens, J.K., McMahon, T.B.: Tridentate ionic hydrogen-bonding interactions of the 5-fluorocytosine cationic dimer and other 5-fluorocytosine analogues characterized by IRMPD spectroscopy and electronic structure calculations. *J. Phys. Chem. A* **115**, 9837–9844 (2011)
14. Marta, R.A., McMahon, T.B., Fridgen, T.D.: Infrared multiphoton dissociation spectra as a probe of ion molecule reaction mechanism: the formation of the protonated water dimer via sequential bimolecular reactions with 1,1,3,3-tetrafluorodimethyl ether. *J. Phys. Chem. A* **111**, 8792–8802 (2007)
15. Wu, R.H., McMahon, T.B.: Infrared multiple photon dissociation spectroscopy as structural confirmation for GlyGlyGlyH(+) and AlaAlaAlaH(+) in the gas phase. Evidence for amide oxygen as the protonation site. *J. Am. Chem. Soc.* **129**, 11312 (2007)
16. Wu, R.H., McMahon, T.B.: An investigation of protonation sites and conformations of protonated amino acids by IRMPD spectroscopy. *Chem. Phys. Chem.* **9**, 2826–2835 (2008)
17. Fridgen, T.D.: Infrared consequence spectroscopy of gaseous protonated and metal ion cationized complexes. *Mass Spectrom. Rev.* **28**, 586–607 (2009)
18. Rajabi, K., Theel, K., Gillis, E.A.L., Beran, G., Fridgen, T.D.: The Structure of the protonated adenine dimer by infrared multiple photon dissociation spectroscopy and electronic structure calculations. *J. Phys. Chem. A* **113**, 8099–8107 (2009)
19. Rizzo, T.R., Stearns, J.A., Boyarkin, O.V.: Spectroscopic studies of cold, gas-phase biomolecular ions. *Int. Rev. Phys. Chem.* **28**, 481–515 (2009)
20. Stearns, J.A., Seaiby, C., Boyarkin, O.V., Rizzo, T.R.: Spectroscopy and conformational preferences of gas-phase helices. *Phys. Chem. Chem. Phys.* **11**, 125–132 (2009)
21. Wu, R.H., McMahon, T.B.: Protonation sites and conformations of peptides of glycine [Gly(1-5)H(+)] by IRMPD Spectroscopy. *J. Phys. Chem. B* **113**, 8767–8775 (2009)
22. Drayss, M.K., Armentrout, P.B., Oomens, J., Schaefer, M.: IR spectroscopy of cationized aliphatic amino acids: stability of charge-solvated structure increases with metal cation size. *Int. J. Mass Spectrom.* **297**, 18–27 (2010)
23. Gillis, E.A.L., Fridgen, T.D.: The hydrated Li(+)-adenine-thymine complex by IRMPD spectroscopy in the N-H/O-H stretching region. *Int. J. Mass Spectrom.* **297**, 2–8 (2010)
24. Marta, R.A., Wu, R.H., Eldridge, K.R., Martens, J.K., McMahon, T.B.: Infrared vibrational spectra as a structural probe of gaseous ions formed by caffeine and theophylline. *Phys. Chem. Chem. Phys.* **12**, 3431–3442 (2010)
25. Mino, W.K., Szczepanski, J., Pearson, W.L., Powell, D.H., Dunbar, R.C., Eyler, J.R., Polfer, N.C.: Vibrational signatures of zwitterionic and charge-solvated structures for alkaline earth-tryptophan dimer complexes in the gas phase. *Int. J. Mass Spectrom.* **297**, 131–138 (2010)
26. Prell, J.S., Flick, T.G., Oomens, J., Berden, G., Williams, E.R.: Coordination of trivalent metal cations to peptides: results from IRMPD spectroscopy and theory. *J. Phys. Chem. A* **114**, 854–860 (2010)
27. Rajabi, K., Gillis, E.A.L., Fridgen, T.D.: Structures of alkali metal ion–adenine complexes and hydrated complexes by IRMPD spectroscopy and electronic structure calculations. *J. Phys. Chem. A* **114**, 3449–3456 (2010)
28. Semrouni, D., Balaj, O.P., Calvo, F., Correia, C.F., Clavaguera, C., Ohanessian, G.: Structure of sodiated octa-glycine: IRMPD spectroscopy and molecular modeling. *J. Am. Soc. Mass Spectrom.* **21**, 728–738 (2010)
29. Dunbar, R.C., Steill, J.D., Oomens, J.: Encapsulation of metal cations by the PhePhe ligand: a cation-pi ion cage. *J. Am. Chem. Soc.* **133**, 9376–9386 (2011)

30. Dunbar, R.C., Steill, J.D., Oomens, J.: Chirality-induced conformational preferences in peptide-metal ion binding revealed by IR spectroscopy. *J. Am. Chem. Soc.* **133**, 1212–1215 (2011)

31. Ortega, J.M., Glotin, F., Prazeres, R.: Extension in far-infrared of the CLIO free-electron laser. *Infrared Phys. Technol.* **49**, 133–138 (2006)

32. Frisch, M.J., Trucks, G.W., Schlegel, H.B., Scuseria, G.E., Robb, M.A., Cheeseman, J.R., Scalmani, G., Barone, V., Mennucci, B., Petersson, G.A., Nakatsuji, H., Caricato, M., Li, X., Hratchian, H.P., Izmaylov, A.F.J., Bloino, G.Z., Sonnenberg, J.L., Hada, M., Ehara, M., Toyota, K., Fukuda, R., Hasegawa, J., Ishida, M., Nakajima, T., Honda, Y., Kitao, O., Nakai, H., Vreven, T., Montgomery Jr., J.A., Peralta, J.E., Ogliaro, F., Bearpark, M., Heyd, J.J., Brothers, E., Kudin, K.N., Staroverov, V.N., Kobayashi, R., Normand, J., Raghavachari, K., Rendell, A., Burant, J.C., Iyengar, S.S., Tomasi, J., Cossi, M., Rega, N., Millam, J.M., Klene, M., Knox, J.E., Cross, J.B., Bakken, V., Adamo, C., Jaramillo, J., Gomperts, R., Stratmann, R.E., Yazyev, O., Austin, A.J., Cammi, R., Pomelli, C., Ochterski, J.W., Martin, R.L., Morokuma, K., Zakrzewski, V.G., Voth, G.A., Salvador, P., Dannenberg, J.J., Dapprich, S., Daniels, A.D., Farkas, O., Foresman, J.B.J.V., Ortiz, J.C., Fox, D.J.: Gaussian 09, Revision A. 02. Gaussian, Inc, Wallingford (2009)

33. Carl, D.R., Cooper, T.E., Oomens, J., Steill, J.D., Armentrout, P.B.: Infrared multiple photon dissociation spectroscopy of cationized methionine: effects of alkali-metal cation size on gas-phase conformation. *Phys. Chem. Chem. Phys.* **12**, 3384–3398 (2010)

34. Armentrout, P.B., Rodgers, M.T., Oomens, J., Steill, J.D.: Infrared multiphoton dissociation spectroscopy of cationized serine: effects of alkali-metal cation size on gas-phase conformation. *J. Phys. Chem. A* **112**, 2248–2257 (2008)

35. Cooper, T.E., Carl, D.R., Oomens, J., Steill, J.D., Armentrout, P.B.: Infrared spectroscopy of divalent zinc and cadmium crown ether systems. *J. Phys. Chem. A* **115**, 5408–5422 (2011)

36. Dunbar, R.C., Steill, J.D., Oomens, J.: Conformations and vibrational spectroscopy of metal-ion/polylalanine complexes. *Int. J. Mass Spectrom.* **297**, 107–115 (2010)

37. Andersson, M.P., Uvdal, P.: New scale factors for harmonic vibrational frequencies using the B3LYP density functional method with the triple-xi basis set 6–311+G(d, p). *J. Phys. Chem. A* **109**, 2937–2941 (2005)

38. Barone, V.: Vibrational zero-point energies and thermodynamic functions beyond the harmonic approximation. *J. Chem. Phys.* **120**, 3059–3065 (2004)

39. Clabo Jr., D.A., Allen, W.D., Remington, R.B., Yamaguchi, Y., Schaefer III, H.F.: A systematic study of molecular vibrational anharmonicity and vibration-rotation interaction by SCF higher-derivative methods. Asymmetric top Molecules. *Chem. Phys.* **123**, 187–239 (1988)

40. CRC Handbook of Chemistry and Physics. Cleavland, Ohio: The Chemical Rubber Co. (1971)

41. Gardner, M., Li, N., Ellington, A., Brodbelt, J.: Infrared multiphoton dissociation of small-interfering RNA anions and cations. *J. Am. Soc. Mass Spectrom.* **21**, 580–591 (2010)

42. Surjasasmita, P.I., Freiser, B.S.: Collision-induced and infrared multiphoton dissociation studies on M(acetone)2+ (M=A1, Fe, Co, Cu, ScO) in the gas phase. *J. Am. Soc. Mass Spectrom.* **4**, 135–144 (1993)

43. Parr, C., Brodbelt, J.S.: Increased sequence coverage of thymine-rich oligodeoxynucleotides by infrared multiphoton dissociation compared to collision-induced dissociation. *J. Mass Spectrom.* **45**, 1098–1103 (2010)